



## Regular Article

## Magnéli phase titanium suboxides by Flash Spark Plasma Sintering

Min Yu<sup>a,b</sup>, Theo Saunders<sup>a,b</sup>, Salvatore Grasso<sup>a,b</sup>, Amit Mahajan<sup>a,b</sup>,  
Hangfeng Zhang<sup>a</sup>, Mike John Reece<sup>a,b,\*</sup>

<sup>a</sup> School of Engineering and Material Science, Queen Mary University of London, London E1 4NS, UK

<sup>b</sup> Nanoforce Technology Limited, London E1 4NS, UK

## ARTICLE INFO

## Article history:

Received 9 November 2017

Accepted 23 November 2017

Available online xxxx

## Keywords:

Flash Spark Plasma Sintering

Magnéli phase

Electrical conductivity

## ABSTRACT

A Flash Spark Plasma Sintering (FSPS) technique was used to fully densify Magnéli phase titanium suboxides (95%TD) in 9 s. A modified FSPS setup contributed to produce homogeneous and dense microstructures, thus avoiding undesired residual porosity at the contact surfaces between samples and electrodes. FSPSed samples retained the original phases ( $\text{Ti}_4\text{O}_7$ ,  $\text{Ti}_5\text{O}_9$  and  $\text{Ti}_6\text{O}_{11}$ ) of the starting powder, whereas  $\text{Ti}_4\text{O}_7$  disappeared in those samples densified using Conventional Spark Plasma Sintering (CSPS). Compared to CSPSed samples, FSPSed ones possessed higher room-temperature electrical conductivity ( $1558 \text{ S} \cdot \text{cm}^{-1}$ ). FSPSed sample exhibited good thermoelectric properties with a figure of merit (ZT) of 0.085 at 1073 K.

© 2017 Acta Materialia Inc. Published by Elsevier Ltd. This is an open access article under the CC BY license (<http://creativecommons.org/licenses/by/4.0/>).

Flash sintering (FS) is a promising and energy-saving sintering technique that can densify particulate materials in a few seconds at much lower temperatures than using conventional sintering. During the past six years, Flash Sintering (FS) has been applied to densify a wide range of materials, including ionic conductors (i.e.  $\text{Y}_2\text{O}_3$ -doped  $\text{ZrO}_2$  [1],  $\text{Ce}_{0.8}\text{Gd}_{0.2}\text{O}_{1.9}$  [2],  $\text{Co}_2\text{MnO}_4$  [3]), semiconductors and insulators (i.e.  $\text{SnO}_2$  [2],  $\text{TiO}_2$  [4],  $\text{ZnO}$  [5],  $\text{BaTiO}_3$  [6] and  $\text{KNbO}_3$  [7],  $\text{SiC}$  [8],  $\text{B}_4\text{C}$  [9],  $\text{SrTiO}_3$  [10],  $\text{Al}_2\text{O}_3$  [11]), as well as several metallic like non-oxide ceramics (i.e.  $\text{ZrB}_2$  and  $\text{MoSi}_2$ ) [12–14]. However, the typical geometry for FSed samples is a dog-bone shape, which has little practical application, and preheating of materials with low electrical conductivity is also required to initiate FS. Flash Spark Plasma Sintering (FSPS) has been proposed to avoid the limitation in geometry and the requirement of preheating [13]. It simply involves using Spark Plasma Sintering equipment without the use of a die so that all of the electrical current passes directly through the sample.

An obvious difference in microstructures between the core and border of fractured FSed samples has been generally observed [15,16]. This heterogeneous microstructure probably results from heat loss at the surface by radiation during sintering, polarity induced effects [16], or uneven current flow caused by non-homogeneity of packed particles in the bulk of samples [14,17]. The aim of this work was to obtain homogeneous microstructures in titanium suboxides using FSPS with a newly developed setup.

Ceramics with Magnéli phase with the general formula  $\text{Ti}_n\text{O}_{2n-1}$  ( $n = 4\text{--}10$ ) are of great interest due to their excellent electrical

conductivity and corrosion resistance. The electrical conductivity of these Magnéli phases decreases with increasing  $n$  value (4–8), ranging from 1995 to  $25 \text{ S} \cdot \text{cm}^{-1}$  [18]. They are extrinsic  $n$ -type semiconductors.  $\text{Ti}_4\text{O}_7$ , a Magnéli phase with  $n = 4$ , possesses the highest electrical conductivity of the homologous series of 1995  $\text{S} \cdot \text{cm}^{-1}$  at room-temperature, compared to other phases ( $631 \text{ S} \cdot \text{cm}^{-1}$  for  $\text{Ti}_5\text{O}_9$ ,  $63 \text{ S} \cdot \text{cm}^{-1}$  for  $\text{Ti}_6\text{O}_{11}$ ,  $25 \text{ S} \cdot \text{cm}^{-1}$  for  $\text{Ti}_8\text{O}_{11}$ ) [18]. Based on their superior electrical conductivity and electrochemical stability, titanium suboxides have been generally applied as promising candidates for electrochemical applications, including catalyst coated materials [19], fuel cells [20], bipolar batteries [21], and environmental treatment [22].

Zhang et al. [23] densified titanium suboxides ( $\text{Ti}_4\text{O}_7$ ) powders with particle size of 1–2  $\mu\text{m}$  to nearly full density at 900 °C with an axial pressure of 40 MPa using Spark Plasma Sintering (SPS). However, the  $\text{Ti}_4\text{O}_7$  phase was completely oxidised into  $\text{Ti}_5\text{O}_9$  even in the vacuum conditions used during the SPS processing.  $\text{Ti}_4\text{O}_7$  powders with an average particle size of 1–3  $\mu\text{m}$  have been densified to 70.3% (relative density) at 700 °C and 30 MPa by SPS [24]. In this work, we report for the first time densification of Magnéli phase titanium suboxides powders by FSPS, aiming to retain the  $\text{Ti}_4\text{O}_7$  phase of the raw powders and achieve uniform microstructures in the sintered samples.

In this paper, FSPS was applied to fully densify titanium suboxides ceramic powders with agglomerates ranging from 50 to 500  $\mu\text{m}$ . The effects of temperature and SPS duration time on microstructures (i.e. homogeneity, grain size) and phase transition between Magnéli phases ( $\text{Ti}_n\text{O}_{2n-1}$ ) during sintering was studied. Samples were also prepared using Conventional Spark Plasma Sintering (CSPS) to compare with the samples prepared using the modified FSPS arrangement. It is first time that the room-temperature (RT) electrical conductivity and thermoelectric property of FSPSed samples have been reported.

\* Corresponding author at: Nanoforce Technology Limited Joseph Priestley Building, Queen Mary, University of London, Mile End Road, London E1 4NS, UK.  
E-mail address: [m.j.reece@qmul.ac.uk](mailto:m.j.reece@qmul.ac.uk) (M.J. Reece).

Titanium suboxide ( $\text{Ti}_n\text{O}_{2n-1}$ ) powders containing the agglomerates (diameter: 50 to 500  $\mu\text{m}$ ) was used as the starting material. The green bodies with the relative density of  $\sim 50.1\%$ , were prepared under a uniaxial pressure of 16 MPa at 1000  $^\circ\text{C}$  for 3 min using a SPS device (FCT HPD 25; FCT Systeme GmbH, Rauenstein, Germany) under vacuum (5 Pa). The heating/cooling rate of this process was 100  $^\circ\text{C}/\text{min}$ .

In the FSPS configuration (Fig. 1), the prepared green body was surrounded by electrically insulating alumina paper rings with outer diameter of 40 mm and pressed between two graphite papers (Sigraflex® graphite foil) by graphite punches ( $\varnothing = 40$  mm). Two kinds of FSPS setups were applied to sinter samples, without (Fig. 1a) and with (Fig. 1b) porous graphite felt (Sigratherm GFA,  $\varnothing = 40$  mm), respectively. No graphite die was employed in the FSPS process, so that the entire current flowed through the sample, which is a common feature of FS.

In order to investigate the densification behaviour of the powders and to make a comparison with the FSPSed samples, CSPSed samples were also prepared using different temperatures (1300–1500  $^\circ\text{C}$ ) and duration times (5–15 min).

The morphologies of samples were observed using a scanning electron microscope (FEI, Inspect F, Hillsboro, OR). The density of samples was determined by measuring the weight and dimensions of bulk samples. X-ray diffraction (XRD) was applied to measure the phases of the samples using Cu K $\alpha$  radiation (Siemens Diffraktometer-D5000, Munich, Germany). The theoretical density (TD) of the raw powder was estimated to be 4.30 g/cm<sup>3</sup>. The grain size of the samples was measured on polished cross sections after being thermally etched at 1000  $^\circ\text{C}$ . The room-temperature electrical conductivity of samples was measured by two-point conductivity measurement with a combination of a picoammeter (Keithley 6485) and DC voltage source (Agilent 6614C). Atomic Force Microscopy (AFM, NT-MDT Ntegra) in conducting AFM mode was used to map the electrical conductivity distribution with the application of DC bias on the conducting probe (Micromash, HQ:NSC14/Pt). The I–V sweeps were carried on different regions of the samples.

The Seebeck coefficient ( $s$ ) and electrical resistivity ( $\rho$ ) were measured on bar samples ( $2 \times 3 \times 6$  mm) using a Linseis LSR-3 with Pt thermocouples and electrodes, with the temperature ( $T$ ) ranging from 300 K to 1073 K. The thermal diffusivity ( $\alpha$ ) was measured on cubic samples

( $6 \times 6 \times 1.3$  mm) using a LFA-457, Netzsch. The specific heat capacity ( $C_p$ ) of the samples was calculated using the Dulong-Petit equation. The thermal conductivity ( $\kappa$ ) was calculated using the following equation:  $\kappa = C_p \times D \times \alpha$ . The power factor (PF) and merit of figure (ZT) were calculated using  $\text{PF} = s^2/\rho$ ,  $\text{ZT} = \text{PF} \cdot T/\kappa$ , respectively.

Fig. 2 shows the output data during FSPS processing of the  $\text{Ti}_n\text{O}_{2n-1}$  powders using setups a and b and the corresponding microstructures of the FSPSed samples. Fig. 2a and b shows the piston displacements started to increase rapidly 4 s after the start of a rapid increase of the current densities, and continued for a further period of 5 s. During this short period ( $\sim 9$  s) FS occurred, which is characterized by the rapid piston distance/sample shrinkage. The current densities calculated as current divided by sample cross section for the FSPS using the setups a and b are 6.18 A/mm<sup>2</sup> and 3.47 A/mm<sup>2</sup>, respectively. The high resistance of the porous graphite felt in setup b explains the lower current density for set up b. The piston displacement in setup b was greater than for setup a, indicating a higher sample density in setup b.

Fig. 2 shows the optical (as inset) and SEM micrographs of the fracture surfaces of FSPSed samples prepared using the setups a and b. The surfaces of the samples in contact with the graphite paper obtained using FSPS with setup a (Fig. 1a) showed a porous microstructure (Fig. 2c, depth: 800  $\mu\text{m}$ ), while the center of the sample has a fully dense microstructure (Fig. 2e). This may result from the temperature gradient caused by the heat exchanged at the interface between the graphite paper and the sample. As shown in Fig. 3d and f, dense and homogenous microstructures were observed at the surface and center of samples prepared using setup b (Fig. 1b). The low thermal conductivity of porous graphite felt improved the temperature uniformity of the sample, by reducing heat loss from the interface between the graphite paper and samples, resulting in a more homogenous microstructure (see Fig. 3c and d). In addition, compared to SPSed  $\text{Ti}_4\text{O}_7$  [24], the absence of intragranular pores in the FSPSed samples indicates that no pore boundary separation happened at high temperatures.

Fig. 3 shows that X-ray diffraction (XRD) patterns of the raw powder and FSPSed samples obtained with setup b and CSPSed samples at different temperatures. XRD analysis of the  $\text{Ti}_n\text{O}_{2n-1}$  powders proves the existence of four Magnéli phases with estimated portions of

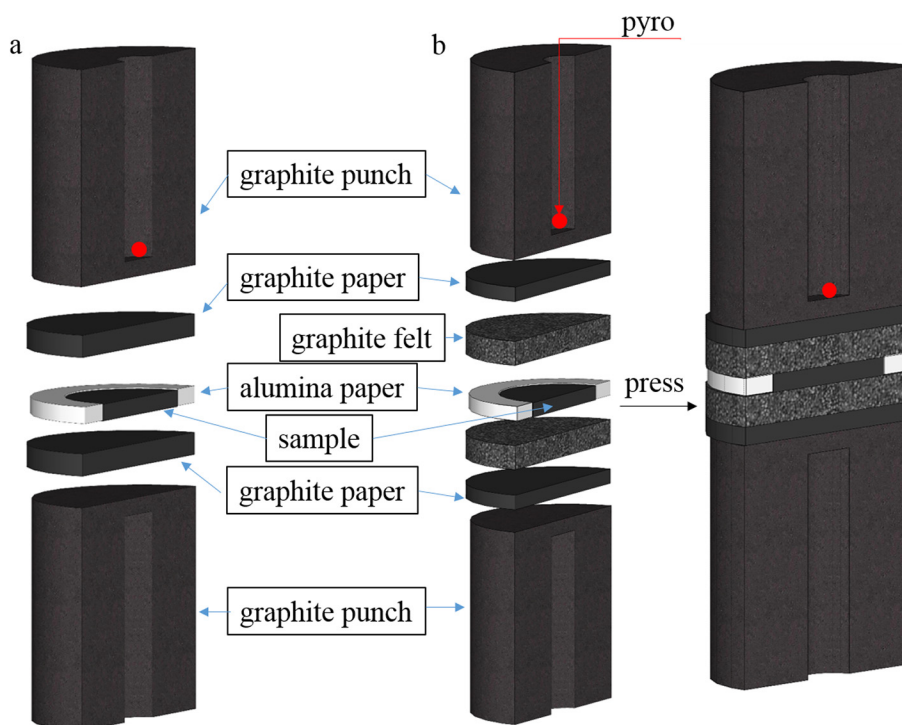
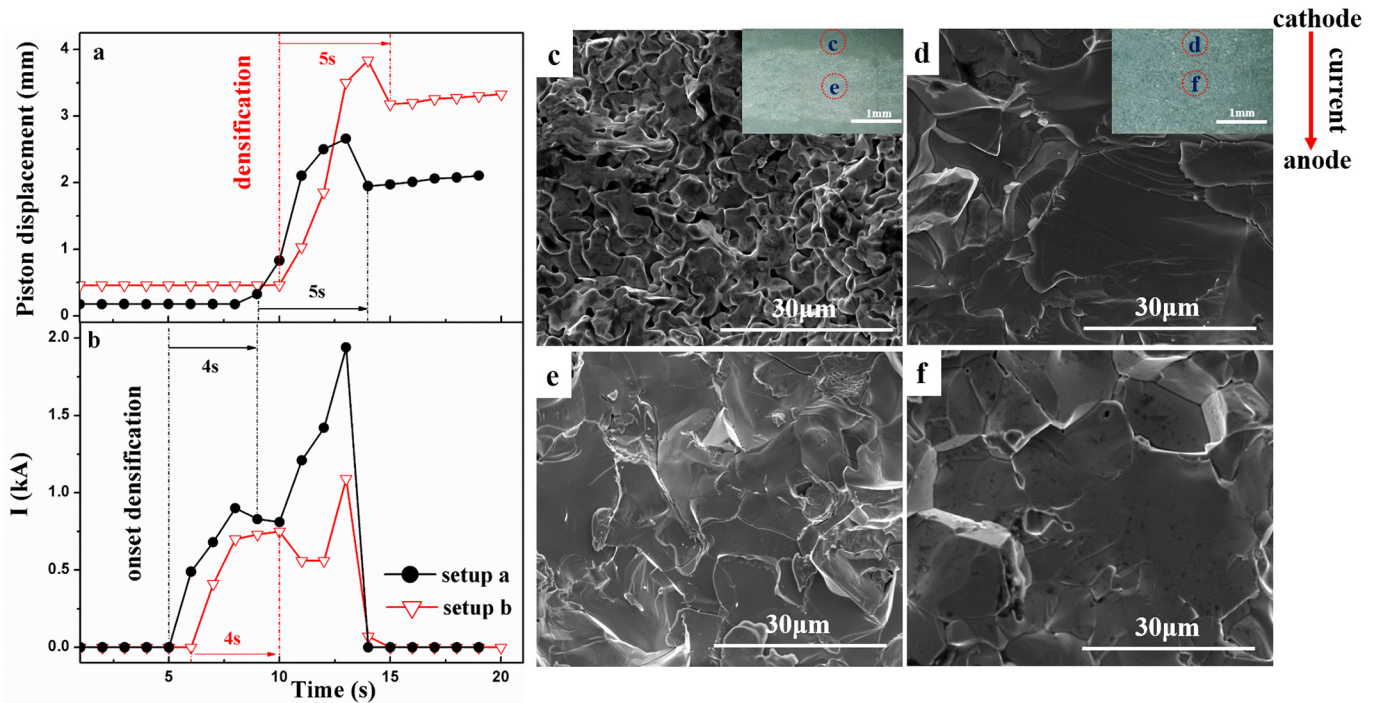


Fig. 1. The experimental setup for FSPS without (a) and with (b) porous graphite felt.



**Fig. 2.** The output data generated during FSPS using the setup a and b: (a) piston displacement; (b) current. SEM of fracture in sintered samples using FSPS without (c and e) and with (d and f) porous graphite felt: fracture edge (a and d) and fracture center (e and f). Inset: optical micrographs of samples.

21.4 wt%  $\text{Ti}_4\text{O}_7$ , 47.6 wt%  $\text{Ti}_5\text{O}_9$  and 31.0 wt%  $\text{Ti}_6\text{O}_{11}$ . The XRD pattern of the FSPSed sample is nearly the same as that of the raw powders, indicating that little transformation between the four Magnéli phases occurred during the FSPS processing. This is a result of the ultrafast heating rate ( $>5000^\circ\text{C}/\text{min}$ ) and sintering during FSPS. However, the characteristic peak at  $2\theta = 20.7^\circ$  (see red box in Fig. 3) for  $\text{Ti}_4\text{O}_7$  disappeared in the CSPSed samples, indicating that  $\text{Ti}_4\text{O}_7$  phases transformed into  $\text{Ti}_5\text{O}_9$  or  $\text{Ti}_6\text{O}_{11}$  during sintering. This transformation might result from either the oxygen contamination or oxygen exchange among  $\text{Ti}_n\text{O}_{2n-1}$  phases inside samples. Zhang et al. reported that  $\text{Ti}_4\text{O}_7$  powders with a small amount of impurity can easily transform into  $\text{Ti}_5\text{O}_9$  in vacuum at  $900^\circ\text{C}$  during SPS processing, probably due to the oxygen contamination on the surface of the raw powders [23]. The relevant Ellingham diagram indicates that the effective partial oxygen pressure ( $\text{PO}_2$ ) for the boundary between stoichiometric titania and titanium

suboxides is  $\sim 10^{-10}$ – $10^{-12}$  Pa at  $1000$ – $1500^\circ\text{C}$  [25], which are considerably lower than the oxygen partial pressure of the vacuum of the SPS chamber. The results suggest that the prolonged processing time in CSPS conditions cause a completed oxidation of  $\text{Ti}_4\text{O}_7$  into  $\text{Ti}_5\text{O}_9$  and  $\text{Ti}_6\text{O}_{11}$ , while such reaction was kinetically inhibited in the case of FSPS because of the very short processing time. The surface and center of FSPSed samples exhibited similar XRD patterns as shown in Supplementary Fig. S2. Since ceramics with Magnéli phases have been used as electrode materials [18], FSPS provides a viable route to retain  $\text{Ti}_4\text{O}_7$  with the highest electrical conductivity among all of the Magnéli phases. Recently, FSPS was also found very effective for consolidation of other oxides [27].

Table 1 shows the bulk density, average grain size and electrical conductivity of the samples obtained using FSPS with the setups a and b, and CSPS with different temperatures and duration time. The Magnéli phase  $\text{Ti}_n\text{O}_{2n-1}$  samples obtained using FSPS with the setup b show much higher density ( $4.10\text{ g/cm}^3$ ) than those obtained using CSPS. With the temperature increasing from  $1300$  to  $1500^\circ\text{C}$ , the density of the CSPS samples increased from  $3.32$  to  $3.70\text{ g/cm}^3$ , mainly resulting from removal of large pores inside samples. With the time variation

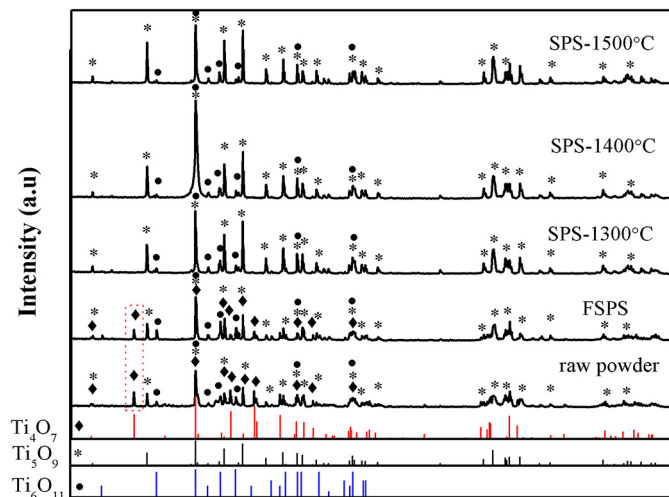


**Fig. 3.** X-ray diffraction patterns of the raw powders and samples sintered in different conditions.

**Table 1**

The bulk density, electrical conductivity, and average grain size of samples obtained using FSPS and CSPS.

Configuration	Duration time	Bulk density ( $\text{g/cm}^3$ )	Electrical conductivity $\sigma$ ( $\text{S}\cdot\text{cm}^{-1}$ )	Grain size ( $\mu\text{m}$ )	
				Fracture center	Contact surface <sup>a</sup>
FSPS-setup a	5 s	–	–	32	–
FSPS-setup b	5 s	4.10	$1558 \pm 23$	32	28
CSPS-1300 $^\circ\text{C}$	0 s	2.59	$576 \pm 19$	–	–
CSPS-1400 $^\circ\text{C}$	0 s	3.32	$882 \pm 21$	–	–
CSPS-1500 $^\circ\text{C}$	0 s	3.70	$1062 \pm 25$	35	57
CSPS-1500 $^\circ\text{C}$	5 min	3.78	–	36	110
CSPS-1500 $^\circ\text{C}$	15 min	3.94	–	36	200

<sup>a</sup> Surface ( $300\mu\text{m}$  in direction parallel to the current flow) of samples contacting with cathode punch (CSPS) or graphite (FSPS).



from 0 to 15 min at 1500 °C in CSPS, the bulk density increased from 3.70 to 3.94 g/cm<sup>3</sup>.

The grain sizes at both the center (~32 μm) and contact surfaces (~28 μm) of the samples obtained using FSPS with setup b only showed a small difference, and remained almost the same as the original grain size (~27 μm) of the raw ceramic powder. In contrast, the grain size in the center of the CSPS samples increased slightly to 36 μm, while the grain size at the sample contact surfaces significantly increased to 200 μm. The significant grain growth at the sample surfaces might result from the carbon diffusion of graphite into sample surface at higher temperatures and longer duration time. In addition, it is quite interesting to observe that longer dwell times at 1500 °C during CSPS resulted in the disappearance of the pores in the CSPS samples without significant additional grain growth (see Supplementary Fig. S1).

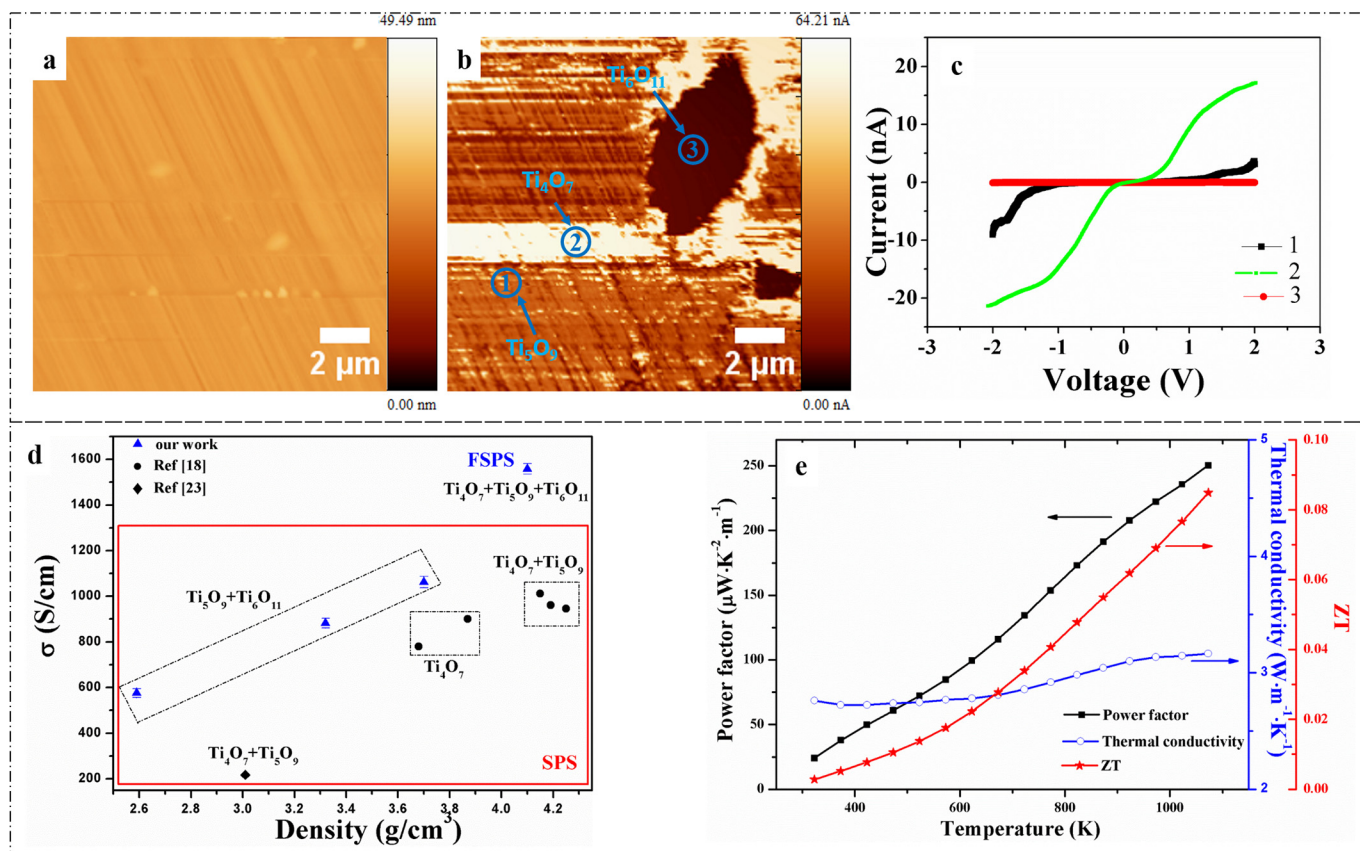
The electrical conductivity of the CSPSed samples increased from 576 to 1062 S·cm<sup>-1</sup> with sintering temperature increasing from 1300 to 1500 °C, mainly a result of increased densification. The FSPSed samples using setup b shows the largest electrical conductivity of 1558 S·cm<sup>-1</sup>, mostly due to the retained Ti<sub>4</sub>O<sub>7</sub> phases and high density.

Fig. 4 shows AFM images and thermoelectric related properties of FSPSed samples obtained using setup b (Fig. 1b), and the electrical conductivity versus bulk density of FSPSed and CSPSed samples. The AFM-topography image (Fig. 4a) of the FSPSed sample further confirmed the dense microstructure obtained by FSPS using setup b. Accordingly, the electric conductivity map (Fig. 4b) was applied to further identify the distribution of different phases (i.e. Ti<sub>4</sub>O<sub>7</sub>, Ti<sub>5</sub>O<sub>9</sub>, Ti<sub>6</sub>O<sub>11</sub>) in the FSPSed sample, owing to the difference in electric conductivity of these phases. The bright and dark regions (Fig. 4c) indicate the highly conductive and resistive regions respectively. The yellow spot 1, bright spot 2 and black spot 3 indicate Ti<sub>5</sub>O<sub>9</sub>, Ti<sub>4</sub>O<sub>7</sub> and Ti<sub>6</sub>O<sub>11</sub>-rich regions, respectively. The corresponding I–V profile for the three regions in Fig. 4b

further confirmed this distribution of Magnéli Ti<sub>n</sub>O<sub>2n-1</sub> phases. The I–V curves from spot 1 and 2 show the variation in the current as a function of voltage of the conductive phases of Ti<sub>5</sub>O<sub>9</sub> and Ti<sub>4</sub>O<sub>7</sub>, respectively, whereas, spot 3 does not show any current flow, indicating the highly resistive Ti<sub>6</sub>O<sub>11</sub> phase. Compared with results of CSPSed samples from the literature, the FSPSed sample exhibited the highest electrical conductivity of 1558 S/cm, owing to the high density and retained Ti<sub>4</sub>O<sub>7</sub> phase (Fig. 4d).

The corresponding power factor reached up to 250 μW·K<sup>-2</sup>·m<sup>-1</sup> at 1073 K, which is half of the reported value (~500 μW·K<sup>-2</sup>·m<sup>-1</sup>) of Magnéli phase titanium suboxide (Ti<sub>4</sub>O<sub>7</sub>) ceramics prepared by Harada [26]. The temperature dependence of the thermal conductivity of FSPSed sample was nearly constant in the temperature range of 323–1073 K, with a value of ~3 W·m<sup>-1</sup>·K<sup>-1</sup>. The merit of figure (ZT) reached up to 0.085 at 1073 K, which is slightly lower than for pure Ti<sub>5</sub>O<sub>9</sub> sample (0.092 at 773 K) prepared by hot pressing [26].

The titanium suboxide powders (Magnéli phase-Ti<sub>n</sub>O<sub>2n-1</sub>) with agglomerates ranging from 50 to 500 μm were densified using FSPS with two types of configuration. Instead of obtaining a porous microstructures on the contact surface between samples and graphite paper found in setup a, homogenous microstructures were obtained in samples prepared using a modified Flash Spark Plasma Sintering (FSPS) technique with porous graphite felt. The rapid sintering process of FSPS contributed to retain the original phases (Ti<sub>4</sub>O<sub>7</sub>, Ti<sub>5</sub>O<sub>9</sub> and Ti<sub>6</sub>O<sub>11</sub>) of the raw powders, while Ti<sub>4</sub>O<sub>7</sub> disappeared in the samples obtained using CSPS. In addition, the room-temperature electrical conductivity of the FSPSed samples (1558 S·cm<sup>-1</sup>) was much higher than those obtained using CSPS. The thermoelectric property of FSPSed sample was investigated, exhibiting a power factor of 250 μW·K<sup>-2</sup>·m<sup>-1</sup>) and merit of figure (ZT) of 0.085 at 1073 K. The effects of different temperatures (1300–1500 °C) and duration times (0–15 min at 1500 °C) in



**Fig. 4.** Topography (a) and electrical conductivity map (b) of FSPSed samples; (c) I–V curves from the spot 1, 2 and 3 (marked by blue circle); (d) Electrical conductivity versus bulk densities of samples obtained by CSPS and FSPS; (e) Temperature-dependent thermal conductivity, power factor and ZT of FSPSed sample. (For interpretation of the references to color in this figure legend, the reader is referred to the web version of this article.)

conventional Spark plasma sintering (CSPS) on the densification of titanium suboxide powders were also investigated. The grain size ( $\sim 200\text{ }\mu\text{m}$ ) of the contact surfaces between sample and graphite punch in CSPS was about 5 times larger than that of the center of the sample.

### Acknowledgement

M.Y. gratefully acknowledge the support of the European Community's Horizon 2020 Programme through a Marie Skłodowska-Curie Innovative Training Network ('CoACH-ETN', <http://www.coach-etn.eu/>, g.a. no. 642557). S.G. was supported by EPSRC (EP/K008749/1, XMat). T.S. was supported by EC FP7 2007–2013 (ADMACOM). MJR would like to acknowledge the support of Sunchon National University, South Korea, through the BK21 + programme.

### Appendix A. Supplementary data

Supplementary data to this article can be found online at <https://doi.org/10.1016/j.scriptamat.2017.11.044>.

### References

- [1] M. Cologna, B. Rashkova, R. Raj, *J. Am. Ceram. Soc.* 93 (11) (2010) 3556–3559.
- [2] A. Gaur, V.M. Sglavo, *J. Am. Ceram. Soc.* 98 (6) (2015) 1747–1752.
- [3] A. Gaur, V.M. Sglavo, *J. Eur. Ceram. Soc.* 34 (10) (2014) 2391–2400.
- [4] S. Jha, J. Lebrun, K. Seymour, W. Kriven, R. Raj, *J. Eur. Ceram. Soc.* 36 (1) (2016) 257–261.
- [5] Y. Zhang, J. Luo, *Scr. Mater.* 106 (2015) 26–29.
- [6] A. Uehashi, K. Sasaki, T. Tokunaga, H. Yoshida, T. Yamamoto, *Microscopy* (Oxford, England) 63 (2014) i19–i20.
- [7] N. Shomrat, S. Baltianski, C.A. Randall, Y. Tsur, *J. Eur. Ceram. Soc.* 35 (7) (2015) 2209–2213.
- [8] S. Grasso, E.-Y. Kim, T. Saunders, M. Yu, S.-H. Choi, A. Tudball, M. Reece, *Cryst. Growth Des.* 16 (4) (2016) 2317–2321.
- [9] B. Niu, F. Zhang, J. Zhang, W. Ji, W. Wang, Z. Fu, *Scr. Mater.* 116 (2016) 127–130.
- [10] A. Karakuscu, M. Cologna, D. Yarotski, J. Won, J.S. Francis, R. Raj, B.P. Uberuaga, *J. Am. Ceram. Soc.* 95 (8) (2012) 2531–2536.
- [11] M. Cologna, J.S. Francis, R. Raj, *J. Eur. Ceram. Soc.* 31 (15) (2011) 2827–2837.
- [12] G. Cabouro, S. Le Gallet, S. Chevalier, E. Gaffet, Y. Grin, F. Bernard, *Powder Technol.* 208 (2) (2011) 526–531.
- [13] S. Grasso, T. Saunders, H. Porwal, O. Cedillos-Barraza, D.D. Jayaseelan, W.E. Lee, M.J. Reece, *J. Am. Ceram. Soc.* 97 (8) (2014) 2405–2408.
- [14] E. Zapata-Solvas, S. Bonilla, P. Wilshaw, R. Todd, *J. Eur. Ceram. Soc.* 33 (13) (2013) 2811–2816.
- [15] S.W. Kim, S.G. Kim, J.I. Jung, S.J.L. Kang, I.W. Chen, *J. Am. Ceram. Soc.* 94 (12) (2011) 4231–4238.
- [16] Y. Zhang, J.-I. Jung, J. Luo, *Acta Mater.* 94 (2015) 87–100.
- [17] R. Muccillo, E. Muccillo, *J. Eur. Ceram. Soc.* 34 (4) (2014) 915–923.
- [18] F. Walsh, R. Wills, *Electrochim. Acta* 55 (22) (2010) 6342–6351.
- [19] K. Scott, H. Cheng, *J. Appl. Electrochem.* 32 (6) (2002) 583–589.
- [20] V. Rashkova, S. Kitova, T. Vitanov, *Electrochim. Acta* 52 (11) (2007) 3794–3803.
- [21] B. May, D.R. Hodgson, Fuel cells and fuel cell plates, Google Patents, 2004.
- [22] G. Chen, E. Betterton, R. Arnold, W. Ela, *J. Appl. Electrochem.* 33 (2) (2003) 161–169.
- [23] X. Zhang, Y. Liu, J. Ye, R. Zhu, *Mater. Lett.* 114 (2014) 34–36.
- [24] J. Ye, G. Wang, X. Li, Y. Liu, R. Zhu, *J. Mater. Sci. Mater. Electron.* 26 (7) (2015) 4683–4690.
- [25] H. Ellingham, *J. Soc. Chem. Ind. Lond.* 63 (5) (1944) 125.
- [26] S. Harada, K. Tanaka, H. Inui, *J. Appl. Phys.* 108 (8) (2010) 083703.
- [27] C. Manière, G. Lee, E.A. Olevsky, *Sci. Reports.* 7 (1) (2017) 15071.